1521-0111/12/8106-788–799$25.00
MOLECULAR PHARMACOLOGY
Copyright © 2012 The American Society for Pharmacology and Experimental Therapeutics
Mol Pharmacol 81:788–799, 2012

Vol. 81, No. 6
76216/3769431

Mode of Peroxisome Proliferator-Activated Receptor γ Activation by Luteolin

Ana C. Puhl, Amanda Bernardes, Rodrigo L. Silveira, Jing Yuan, Jéssica L. O. Campos, Daniel M. Saidemberg, Mario S. Palma, Aleksandra Cvoro, Stephen D. Ayers, Paul Webb, Peter S. Reinach, Munir S. Skaf, and Igor Polikarpov

Instituto de Física de São Carlos, Universidade de São Paulo, São Carlos, SP, Brazil (A.C.P., A.B., J.L.O.C., I.P.); Instituto de Química, Universidade Estadual de Campinas, Campinas, SP, Brazil (R.L.S., M.S.S.); Department of Biological Sciences, College of Optometry, State University of New York, New York, New York (J.Y., P.S.R.); Laboratório de Biologia Estrutural e Zooquímica, CEIS/Departamento de Biologia, Instituto de Biociências, UNESP, Rio Claro, SP, Brazil (D.M.S., M.S.P.); and Genomic Medicine, Methodist Hospital Research Institute, Houston, Texas (A.C., S.D.A., P.W.)

Received October 10, 2011; accepted March 5, 2012

ABSTRACT

The peroxisome proliferator-activated receptor γ (PPARγ) is a target for treatment of type II diabetes and other conditions. PPARγ full agonists, such as thiazolidinediones (TZDs), are effective insulin sensitizers and anti-inflammatory agents, but their use is limited by adverse side effects. Luteolin is a flavonoid with anti-inflammatory actions that binds PPARγ but, unlike TZDs, does not promote adipocyte differentiation. However, previous reports suggested variously that luteolin is a PPARγ agonist or an antagonist. We show that luteolin exhibits weak partial agonist/antagonist activity in transfections, inhibits several PPARγ target genes in 3T3-L1 cells (*LPL*, *ORL1*, and *CEBPα*) and PPARγ-dependent adipogenesis, but activates *GLUT4* to a similar degree as rosiglitazone, implying gene-specific partial agonism. The crystal structure of the PPARγ ligand-binding domain (LBD) reveals that luteolin occupies a buried ligand-binding pocket (LBP) but binds an inactive PPARγ LBD conformer and occupies a space near the β-sheet region far from the activation helix (H12), consistent with partial agonist/antagonist actions. A single myristic acid molecule simultaneously binds the LBP, suggesting that luteolin may cooperate with other ligands to bind PPARγ, and molecular dynamics simulations show that luteolin and myristic acid cooperate to stabilize the Ω-loop among H2′, H3, and the β-sheet region. It is noteworthy that luteolin strongly suppresses hypertonicity-induced release of the pro-inflammatory interleukin-8 from human corneal epithelial cells and reverses reductions in transepithelial electrical resistance. This effect is PPARγ-dependent. We propose that activities of luteolin are related to its singular binding mode, that anti-inflammatory activity does not require H12 stabilization, and that our structure can be useful in developing safe selective PPARγ modulators.

Introduction

Peroxisome proliferator-activated receptors (PPARs) are ligand-activated transcription factors of the nuclear receptor family. The three PPAR subtypes (PPARα, PPARβ, and PPARγ) have different ligand specificity and tissue distribution (Berger and Moller, 2002). PPARγ is highly expressed in adipose tissue, macrophages, and cells of the vasculature (Tontonoz et al., 1994; Ricote et al., 1998), plays essential roles in adipogenesis and glucose and lipid homeostasis (Auwerx, 1999; Lehrke and Lazar, 2005), and exhibits anti-inflammatory actions (Ricote and Glass, 2007). PPARγ agonists such as the thiazolidinediones (TZDs) are efficient and clinically useful insulin sensitizers and are under investigation for the treatment of inflammation with potential applications in atherosclerosis (Koshiyama et al., 2001), inflammatory colitis (Lewis et al., 2001), arthritis (Giaginis et al., 2009), and bowel disease (Borniquel et al., 2010). PPAR may also be a useful target in ocular conditions. For example,

This work was supported by Fundação de Amparo a Pesquisa do Estado de São Paulo (FAPESP) [Grant 2007/58443-4 and 2010/08680-2] and Coordenação de Aperfeiçoamento de Pessoal de Nível Superior (CAPES).

The atomic coordinates and structure factors of the PPARγ crystal structure reported here were deposited in the Protein Data Bank under code 3SZ1.

Article, publication date, and citation information can be found at http://molpharm.aspetjournals.org.
http://dx.doi.org/10.1124/mol.111.076216.

ABBREVIATIONS: PPAR, peroxisome proliferator-activated receptor; TZD, thiazolidinedione; TEER, transepithelial electrical resistance; LBD, ligand-binding domain; LBP, ligand-binding pocket; FBS, fetal bovine serum; SPPARγM, selective PPARγ modulator; HCEC, human corneal epithelial cell; IL-8, interleukin 8; CEBPα, CCAT enhancer binding protein α; LPL, lipoprotein lipase; ORL1, oxidized LDL receptor 1; GAL4, regulator of gene expression for the galactose-induced genes; DMEM, Dulbecco's modified Eagle's medium; PCR, polymerase chain reaction; PDB, Protein Data Bank; MD, molecular dynamics; ELISA, enzyme-linked immunosorbent assay; H, helix; GW9662, 2-chloro-5-nitro-*N*-4-phenylbenzamide.

dry-eye disease can result in tears with increased osmolarity, which can lead to breaches of the tight junctional barrier property of the corneal epithelium, resulting in an innate immune response, triggered by IL-8 release by corneal epithelium and the underlying stroma, and reductions in transepithelial electrical resistance (TEER) (Luo et al., 2005; Li et al., 2006). PPARγ activation by endogenous metabolites formed in response to severe corneal injury in mice improves the wound-healing response to injury and reduces inflammation and fibrosis (Saika et al., 2007).

Like other nuclear receptors, PPARγ consists of three domains: the N-terminal domain, the DNA-binding domain, and the ligand-binding domain (LBD). The ability of PPARγ to promote or suppress the transcription of responsive genes depends on interaction of its LBD with ligands that stabilize receptor conformation. Full agonists, such as the TZDs, efficiently stabilize C-terminal H12, part of a coactivator binding cleft (activation function 2), allowing efficient recruitment of transcriptional coactivators (Berger and Moller, 2002). The PPARγ ligand-binding pocket (LBP) is a large Y-shaped hydrophobic cavity (Nolte et al., 1998) with a volume almost twice that of LBPs of other nuclear receptors (Zoete et al., 2007) that can accommodate compounds such as fatty acids, arachidonic acid metabolites (Kliewer et al., 1995), antidiabetes drugs (Lehmann et al., 1995), and nonsteroidal anti-inflammatory drugs (Lehmann et al., 1997) with different binding modes (Itoh et al., 2008).

Although TZDs are efficient insulin sensitizers, their use is associated with increased fat mass (Larsen et al., 2003), renal fluid retention, and more severe cardiovascular events (Mudaliar et al., 2003; Nissen and Wolski, 2007). Thus, effort has been directed toward developing efficacious selective PPARγ modulators (SPPARγMs) that improve insulin sensitivity and combat inflammation without inducing other harmful effects (Berger et al., 2003; Higgins and Depaoli, 2010). Partial agonists that occupy positions within the LBP near the β-sheets enhance insulin sensitivity without harmful side effects by inhibiting PPARγ LBD phosphorylation by the proinflammatory kinase cyclin-dependent kinase 5 (Choi et al., 2010; Choi et al., 2011). Thus, alternate PPARγ ligand binding modes may be associated with altered, and potentially useful, spectrums of action relative to full agonists.

The flavonoids, naturally occurring plant polyphenols, display a remarkable array of biochemical and pharmacological actions (Havsteen, 2002). Among them, luteolin (3′,4′,5,7-tetrahydroxyflavone), present in celery, green pepper, perilla leaf, and chamomile tea, is a PPARγ ligand with antioxidant and anti-inflammatory properties (Xagorari et al., 2001). Different studies, however, have suggested that luteolin can function either as a PPARγ agonist [enhances expression of PPARγ-dependent genes in adipocytes (Ding et al., 2010)] or a PPARγ antagonist [inhibits adipogenesis and PPARγ-dependent gene expression in other contexts (Mueller et al., 2008; Park et al., 2009)]. The fact that the mode of luteolin action is unclear prompted us to determine the mechanism of luteolin interaction with PPARγ and the biological relevance of such an effect in inflammatory response in human corneal epithelial cells (HCECs).

Here, we show that luteolin is a PPARγ partial agonist, explaining discrepancies in previous reports about its actions, and combined use of X-ray crystallography and molecular dynamics studies revealed a unique binding mode in which it binds to an inactive PPARγ LBD conformer in a position within the LBP that lies near the β-sheet region of the LBP. The luteolin binding mode permits the simultaneous presence of a long-chain fatty acid in the pocket, and simulations suggest that both ligands cooperate to stabilize the LBD in a different manner from full agonists. In hypertonicity-stressed HCECs, luteolin selectively suppressed release of a chemoattractant, IL-8, and reversed reductions in TEER, suggesting that this unique binding mode is associated with useful anti-inflammatory activities in cornea.

Materials and Methods

Cell Transactivation Assays. Plasmids used were pGRE-LUC (GAL4-responsive element, firefly luciferase reporter vector), the PPARγ LBD-GAL4 inserted in pBIND plasmid (Promega, Madison, WI), and the pRL-TK, which contains *Renilla reniformis* luciferase (Dual-Luciferase Report Assay system; Promega) and was used as transfection control. HepG2 cells were maintained in Dulbecco's modified Eagle's medium (DMEM) supplemented with 10% (v/v) fetal bovine serum, 2 mM glutamine, 50 units/ml penicillin, and 50 mg/ml streptomycin under a 95% air/5% CO_2 atmosphere at 37°C. For transfection, cells were trypsinized, resuspended in DMEM, plated in 24-well plates (density of 1.2×10^5 cells/well), and incubated with 50 ng of pGRE-LUC, 100 ng of PPARγ LBD-GAL4 vector, and 1 ng of pRL-TK, which were incubated with FuGENE (Roche, Indianapolis, IN) at a ratio of 1 μg of DNA to 3 μl of FuGENE at room temperature for 20 min before addition to cells. PPARγ ligands [rosiglitazone (as a control) and luteolin] were added to culture medium 24 h later and incubated with the cells overnight. The cell monolayer was washed with phosphate-buffered saline and harvested with lysis buffer (Dual-Luciferase Report Assay system; Promega) according to the manufacturer's instructions. Luciferase activity was determined using the Luciferase Assay System (Promega) and measured in a Safire 2 luminescent counter (Tecan US, Durham, NC). The *R. reniformis* luciferase activity was measured using the same cell lysate and used as an internal control. The EC_{50} value was calculated using a sigmoidal dose-response function from plots of the relationship between luminescence and luteolin concentrations ($10^{-}9$ to 10^{-5} M), considering the following function: $Y = \text{Bottom} + (\text{Top} - \text{Bottom})/(1 + 10^{(\text{LogEC}_{50} - X)})$, where X is the logarithm of concentration and Y is the response. These analyses were performed with the use of Prism software (version 5.0; GraphPad Software, San Diego, CA).

Cell Culture and Adipocyte Differentiation Assay. Murine 3T3-L1 cells were cultured at 37°C and 5% CO_2 in DMEM, high glucose, and HEPES, pH 7.4, supplemented with 10% FBS, 100 units/ml penicillin, and 100 μg/ml streptomycin. Cells were differentiated to adipocytes as described previously (Klemm et al., 2001). In brief, postconfluent 3T3-L1 cells were maintained in DMEM/Ham's F-12 medium supplemented with 10% FBS, 1 μM dexamethasone, 0.5 mM 3-isobutyl-1-methylxanthine, 167 nM insulin, and 1 μM rosiglitazone for 3 days. The effect of luteolin on rosiglitazone-induced differentiation was assessed by adding 5, 10, or 20 μM luteolin during this period. After 3 days, cells were maintained in DMEM/Ham's F-12 supplemented with FBS, insulin, and dexamethasone until harvesting. On day 8 of differentiation, cells were stained with Oil Red O to estimate in vitro adipogenesis as described previously (Klemm et al., 2001). For gene expression analysis, on day 8 of differentiation, cells were treated as follows: 1) control (no treatment); 2) 10 μM luteolin; 3) 20 μM luteolin; 4) 1 μM rosiglitazone; and 5) 20 μM luteolin and 1 μM rosiglitazone. After 24 h, total RNA was extracted.

Quantitative Real-Time Reverse Transcription-PCR. Total RNA was extracted on day 8 of 3T3-L1 cell differentiation using Aurum Total RNA Fatty and Fibrous kit (Bio-Rad Laboratories, Hercules, CA), in accordance with the manufacturer's instructions. A

total of 160 ng of total RNA was reverse-transcribed using random hexamers and SuperScript III First-Strand Synthesis System for RT-PCR (Invitrogen). Real-time quantitative PCR analysis was performed using SYBR Green PCR Master Mix (Roche), and the following gene specific primers were used: *β-actin*: forward, 5′-GTGACGTTGACATCCGTAAAGA; reverse, 5′-GCCGGACTCATCGTACTCC; *CEBPa*: forward, 5′-GCGGGAACGCAACAACATC; reverse, 5′-GTCACTGGTCAACTCCAGCAC; *LPL*: forward, 5′-GCTGGGCCTAACTTTGAGTATG; reverse, 5′-AAATCAGCGTCATCAGGAGAA; and *OLR1*: forward, 5′-CTGCACTCCTTCTTCCCTTT; reverse, 5-′GCCTGCACTTGAGGAGGATTT. For analysis of *GLUT4* expression, TaqMan real-time PCR was performed using LightCycler 480 Probes Master Mix (Roche) and primers supplied by Applied Biosystems (Foster City, CA). The relative expression of mRNA was determined by normalization to β-actin levels using the $\Delta\Delta C_t$ method. The results were considered to be significant at p values less than 0.05, as measured by Student's t test (paired data).

PPARγ Expression and Purification. The plasmid pET28a(+) (Novagen, Madison, WI) encoding a human PPARγ LBD fused in frame to the C terminus of a polyhistidine (His) tag was used to transform competent *Escherichia coli* strain BL21 (DE3). An initial culture was then inoculated at 1% in a major Luria broth culture and grown at 37°C until $OD_{600\ nm}$ reached 0.8. After this, protein expression was induced with 1 mM isopropyl β-D-thiogalactoside for 16 h at 18°C. Cells were harvested by centrifugation, and the cell pellet was resuspended in 20 mM Tris-HCl, pH 8.0, 500 mM NaCl, 1 mM phenylmethylsulfonyl fluoride, and 1 mM dithiothreitol and incubated on ice with 0.5 mg/ml of lysozyme for 30 min. The cells were disrupted by sonication, and cell debris was removed by centrifugation. The His-tag PPARγ LBD was purified by metal-affinity chromatography from the supernatant using a Talon Superflow Metal Affinity Resin (Clontech, Mountain View, CA). The protein was eluted with stepwise incubations, the lysis buffer containing 100 and 300 mM imidazole, and eluted fractions were pooled and subjected to size-exclusion chromatography (AKTA Purifier System; AKTA Basic; GE Healthcare, Chalfont St. Giles, Buckinghamshire, UK), using Superdex 75 16/60 (GE Healthcare) previously washed and equilibrated with 20 mM TRIS-HCl buffer, pH 8.0, containing 1 mM dithiothreitol, 100 mM NaCl, and 5% glycerol. Samples containing the PPARγ LBD were processed to a final concentration of 10 mg/ml and stored at −80°C. The His-tag was removed by digestion with bovine thrombin (Sigma-Aldrich, St. Louis, MO). The protein content and purity of all chromatographic fractions were analyzed by Coomassie Blue-stained SDS/polyacrylamide gel electrophoresis. Protein concentrations were determined using the Bradford dye assay (Bio-Rad Laboratories) using bovine serum albumin as standard.

Crystallization, Data Collection, and Structure Determination. PPARγ LBD at 10 mg/ml was mixed with 1 mM luteolin on ice and allowed to stand at 4°C overnight. The crystallization screens were preformed under conditions similar to those described previously (Nolte et al., 1998), using hanging drop of 1 μl of protein complex solution mixed with 1 μl of precipitant solution and equilibrated against a 500 ml of reservoir solution containing 100 mM HEPES, pH 7.0 to 8.0, 0.75 to 1.3 M sodium citrate. Suitable crystals were obtained within 2 to 3 days with 100 mM HEPES, pH 7.0, and 0.85 M sodium citrate. Before data collection, the crystals were soaked in a cryoprotectant containing the same reservoir solution added with 15% (v/v) ethylene glycol and rapidly cooled in a gaseous nitrogen stream at 100 K. X-ray diffraction data were collected in the protein crystallography MX2 beamline at the Laboratório Nacional de Luz Síncroton (LNLS, Campinas, Brazil) (Guimarães et al., 2009). Diffraction data were processed using MOSLFM (Leslie, 1999) and scaled with SCALA from the CCP4 program suite (Collaborative Computational Project Number 4, 1994).

The structure was determined by molecular replacement using the program PHASER from CCP4 Packages and the PPARγ LBD (PDB code 2PRG) structure as a model. The programs PHENIX and COOT were used to alternately run cycles of refinement and model building (Emsley and Cowtan, 2004; Adams et al., 2010).

Molecular Dynamics Simulations. For simulations, the missing residues of the crystallographic structure presented in this work (chain B) were completed using coordinates obtained from the chain B of the structure 1PRG (Nolte et al., 1998) of PDB, after structural alignment using the program LovoAlign (Martínez et al., 2007). Modeled residues received special energy minimization treatments before the production runs (see below). The structure was then fully solvated with a water shell of at least 16 Å, and Na^+ and Cl^- ions were added at concentration of 0.15 M to render the system electrically neutral. Short-range interactions were truncated at a cut-off radius of 12 Å, and electrostatic interactions were evaluated via the Particle Mesh Ewald (PME) method, using periodic boundary conditions. After this procedure, PPARγ-luteolin and PPARγ-rosiglitazone complexes were built using the new structure described here and the chain D of the structure 1FM6 of the PDB (Gampe et al., 2000), respectively. The final systems contained around 56,000 atoms.

The CHARMM force field (MacKerell et al., 1998) was used to model the interactions of both the protein and the fatty acid, and the three-site transferable intermolecular potential (TIP3P) model was used for water (Jorgensen et al., 1983). Partial charges for luteolin were obtained via ab initio quantum calculation at RHF/6–31G(d) level using the Merz-Kollman charge adjustment scheme (Singh and Kollman, 1984). Dihedral angle parameters for the torsion around the chemical bond between the two aromatic rings of luteolin were obtained through nonlinear fitting of the quantum potential energy surface obtained at the B3LYP/6–31(d) level, following a protocol similar to that described recently by us (Hansson et al., 2011). The quantum calculations were performed with Gaussian 03 (Frisch et al., 2004). All other force-field parameters for luteolin were obtained by analogy with the CHARMM force field. Force-field parameters for rosiglitazone were obtained previously (Hansson et al., 2011).

Systems were prepared for production runs by 1) 2000 steps of energy minimization using the conjugate gradients algorithm, keeping all atoms of the protein and ligands fixed, except the modeled residues; 2) with the same atoms fixed, 200 ps of molecular dynamics (MD) in the isothermal-isobaric ensemble; 3) 1000 conjugate gradient steps keeping only the Cα fixed; 4) 200 ps of MD in the isothermal-isobaric ensemble, with Cα fixed; and 5) 600 ps of MD without any restraint. The productions runs were 3 ns and the temperature and pressure were set to 300 K and 1 atmosphere, respectively. For each system, this protocol was repeated five times to provide adequate statistical sampling. The simulations were performed with the program NAMD (Phillips et al., 2005).

Enzyme-Linked Immunosorbent Assay. IL-8 release from hypertonic-stressed SV40-immortalized HCECs was measured using an enzyme-linked immunosorbent assay (ELISA; R&D Systems, Minneapolis, MN) as described in the manufacturer's instructions. HCECs were cultured in DMEM/Ham's F12 medium supplemented with 10% FBS, 5 ng/ml epidermal growth factor, 5 μg/ml insulin, and 40 μg/ml gentamicin in a humidified incubator with a 5% CO_2/95% atmosphere air at 37°C. They were transferred to 12-well culture plates and grown until they reached approximately 80% confluence and then exposed to either a PPARγ antagonist [2-chloro-5-nitro-*N*-4-phenylbenzamide (GW9662; Cayman Chemical, Ann Arbor, MI)] or luteolin (Cayman Chemical) for 30 min before exposing them to NaCl-supplemented hypertonic (450 mOsM) DMEM/Ham's F12 medium for 24 h. Supernatants were harvested after centrifugation at 1000 rpm for 5 min to remove cell debris. The supernatants were stored at −80°C until analysis. Protein concentration of each cell lysate was determined by using a bicinchoninic acid protein assay kit (Thermo Scientific). The amount of IL-8 in the culture medium was normalized to the total amount of cellular protein lysed with 5% SDS and 0.5 N NaOH. Results are expressed as mean picograms of IL-8 per milligram of cell protein ± S.E.M. Each experiment was performed in triplicate and repeated three times ($n = 3$). The results

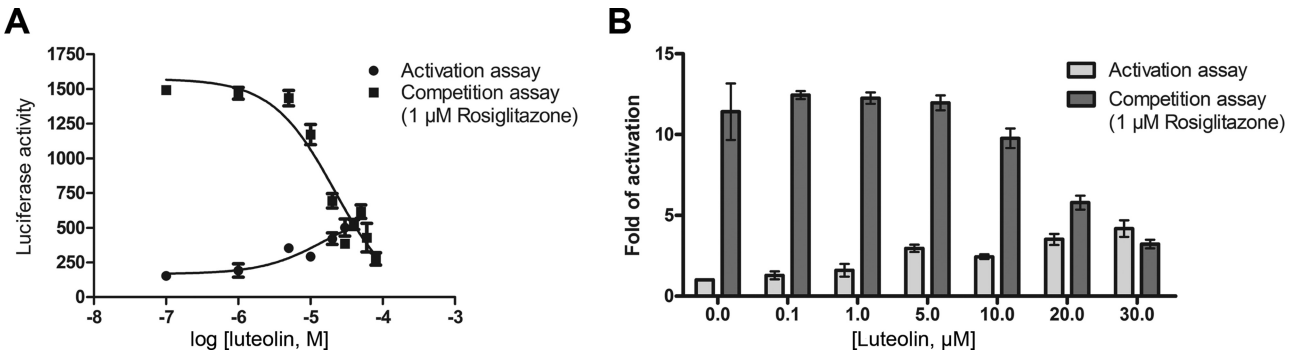

Fig. 1. Cell transactivation assays. PPARγ/GAL4 transactivation assay were performed with serial dilutions of different concentrations of luteolin in activation and competition mode, shown as dose-response curve (A) and fold activation of luciferase (B). Both graphs show the activation and competition with 1 μM rosiglitazone by addition of luteolin. All assays were performed in three replicates and were normalized for differences in transfections efficiency by measuring *R. reniformis* luciferase activity in the same lysate.

were considered to be significant at p values less than 0.05, as measured by Student's t test (paired data).

Transepithelial Electrical Resistance Measurement. For HCEC transepithelial electrical resistance measurements, cells were seeded on Transwell permeable supports having a 24-mm diameter and pore size of 0.4 μm and placed in six-well plates (Corning Life Sciences, Acton, MA) at a density of 5×10^5 cells per well. They were cultured using DMEM/Ham's F12 medium supplemented with 10%

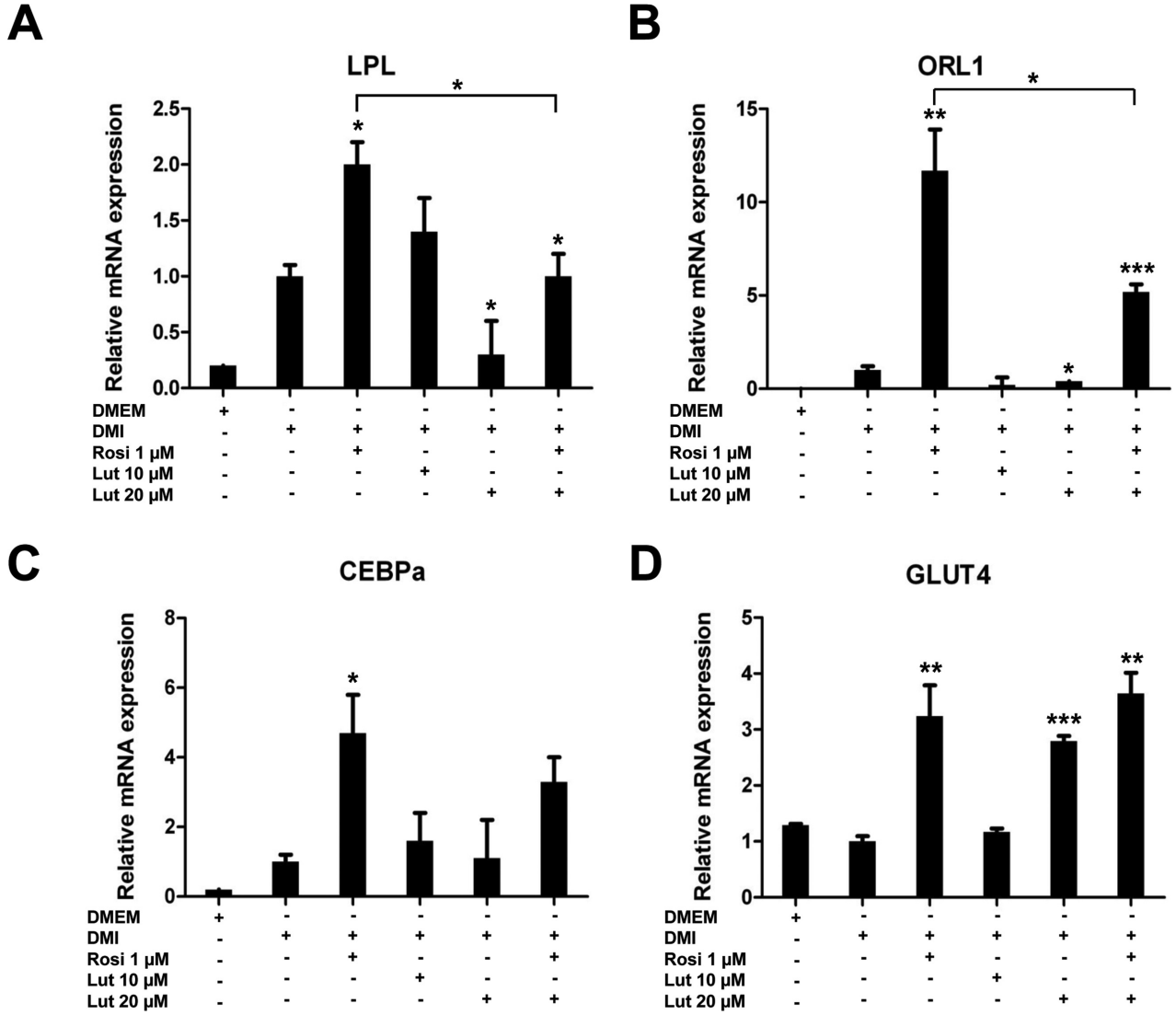

Fig. 2. Quantitative PCR. Quantitative PCR and relative mRNA expression of genes *LPL* (A), *ORL1* (B), *CEBPa* (C), and *GLUT4* (D). 3T3-L1 cells on day 8 of differentiation were exposed to the following treatments: control; 10 μM luteolin (Lut); 20 μM luteolin; 1 μM rosiglitazone (Rosi); and 20 μM luteolin and 1 μM rosiglitazone for 24 h. Each data point is the average of triplicate experiment ± S.D. [*, $P < 0.05$; **, $P < 0.01$; ***, $P < 0.001$ in comparison with 1 μM dexamethasone, 0.5 mM 3-isobutyl-1-methylxanthine, and 167 nM insulin (DMI)].

fetal bovine serum (Invitrogen, Carlsbad, CA). The inserts were air-lifted and exposed to 1 ml of medium in the bottom chamber. After approximately 5 days, the cultures reached confluence based on stable transepithelial electrical resistance values. TEER (ohms per square centimeter) was measured with hand-held electrodes connected to a volt-ohm meter (EVOM; World Precision Instruments, Sarasota, FL) and corrected by subtracting the resistance of an empty insert (Yang et al., 2000).

Results

Luteolin Is a Partial PPARγ Agonist. We performed cell transactivation assays to re-evaluate activity of luteolin relative to rosiglitazone. Dose-response curves obtained with seven different luteolin concentrations are shown in Fig. 1A, where each point represents the mean of three replicates performed in triplicate. Luteolin exhibited moderate, partial agonist-like PPARγ LBD transactivation activity with an EC_{50} of 15.6 μM. The maximal activity achieved by luteolin was 35% of that observed for the full PPARγ agonist rosiglitazone (Fig. 1B). Rosiglitazone response was inhibited by luteolin in a competition assay (Fig. 1B), with an IC_{50} of 21.8 μM, consistent with its partial agonist behavior. Luteolin concentrations greater than 50 μM were cytotoxic, as indicated by the 3-(4,5-dimethylthiazol-2-yl)-2,5-diphenyltetrazolium cell viability assay (data not shown).

Luteolin Regulates PPARγ Target Genes in 3T3-L1 Cells and Inhibits Rosiglitazone-Induced Differentiation. We used quantitative real time PCR to determine whether luteolin regulates expression of PPARγ target genes in 3T3-L1-differentiated cells. After 8 days of differentiation, quantitative real-time PCR was performed on adipocytes treated ± luteolin (10 and 20 μM), rosiglitazone (1 μM), or a combination of these ligands (1 μM rosiglitazone + 20 μM luteolin) for 24 h. As a negative control, we used cells incubated with DMEM instead of standard differentiation medium. As expected, rosiglitazone induced known target genes that regulate fatty acid metabolism and glucose transport such as *LPL*, *ORL1*, *CEBPa*, and *GLUT4* (Morrison and Farmer, 1999; Laplante et al., 2003; Chui et al., 2005; Armoni et al., 2007) (Fig. 2), whereas luteolin actively repressed expression of *LPL* and *OLR1* (Fig. 2, A and B) and did not affect *CEBPα* expression (Fig. 2C). However, luteolin did induce *GLUT4* similarly to rosiglitazone (Fig. 2D). Accordingly, rosiglitazone effects on *LPL*, *OLR1*, and *CEBPa* were inhibited by 20 μM luteolin, whereas expression of *GLUT4* was similar to that in response to rosiglitazone or luteolin alone (Fig. 2). Thus, luteolin behaves as a weak partial agonist/antagonist at several genes in 3T3-L1 cells but also displays full agonist activities at one gene.

Luteolin also inhibited effects of rosiglitazone on adipocyte differentiation. 3T3-L1 cells were treated with 1 μM rosiglitazone in presence of 5, 10, and 20 μM luteolin for 3 days after confluence. On day 8 of differentiation, cells were stained with Oil Red O to verify lipid accumulation. As expected, rosiglitazone triggered efficient differentiation to adipocytes (Fig. 3), and this effect was reversed by luteolin in a dose-dependent manner.

Luteolin and Myristic Acid Simultaneously Bind the PPARγ LBD. To understand the molecular basis of luteolin partial agonism/antagonism, we obtained an X-ray cocrystal structure of the PPARγ LBD with luteolin at 2.3 Å resolution. The structure, solved in the monoclinic C2 space group, shows good geometric and crystallographic parameters and no residues in the disallowed region of the Ramachandran plot (Table 1). In common with previous PPARγ LBD structures, the asymmetric unit contains a homodimer of the PPARγ LBD, with chain A in the canonical active nuclear receptor conformation and chain B in an inactive conformation caused by crystallographic contacts (Nolte et al., 1998). The structure of PPARγ LBD consists of 12 α-helices that form the classic three-layered antiparallel α-helical sandwich

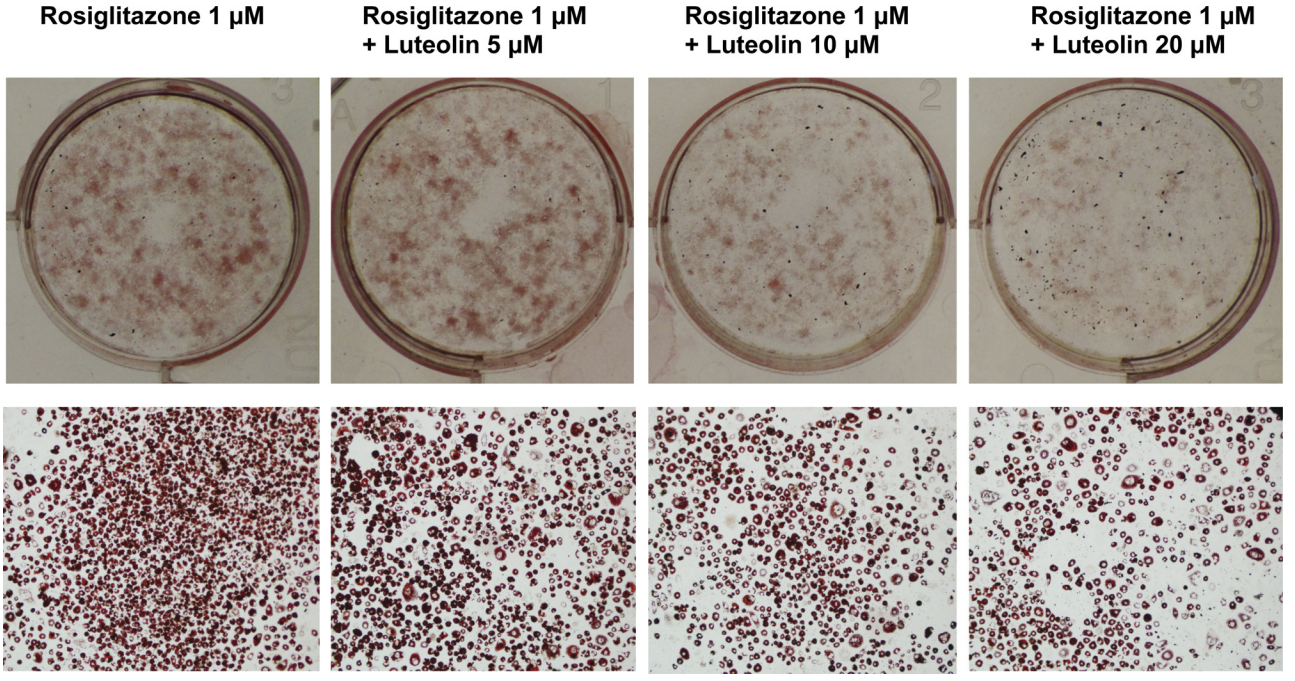

Fig. 3. 3T3-L1 differentiation assay. Oil Red O staining of 3T3-L1 fibroblast cells after differentiating to adipocytes with different ligands for 3 days and maintaining in media with insulin for 8 days. Treatments include 1 μM rosiglitazone, 1 μM rosiglitazone, and 5, 10, or 20 μM luteolin.

TABLE 1
Data collection and structure refinement statistics
Values in parentheses refer to the last resolution shell.

Data Collection	
Space group	C2
Unit cell parameters	
a, Å	92.26
b, Å	62.15
c , Å	119.13
β	101.67
No. of molecules in asymmetric unit	2
Resolution range, Å	31.08–2.3 (2.42–2.3)
Beamline	LNLS MX2
Wavelength, Å	1.4586 Å
Unique reflections	29570
R_{sym}, %	0.079 (0.474)
Multiplicity	7.2 (7.1)
Completeness, %	100 (100)
Mean I/σ(I)	14.3 (3.7)
Bfactor from Wilson plot, Å^2	44
Refinement Statistics	
R_{factor}/R_{free}	0.2066/0.2400
RMS deviation from ideality	
Bond lengths, Å	0.018
Bond angles, °	1.637
Average B-value, Å	
Chain A (258 residues)	52.30
Fatty acids 9 carbons (2 molecules, 22 atoms)	62.14
Solvent (46 molecules)	46.30
Chain B (258 residues)	49.30
Luteolin (1 molecule, 21 atoms)	44.10
Myristic acid (1 molecule, 16 atoms)	54.10
Solvent (52 molecules)	45.70
Ramachandran analysis	
In preferred regions	98.37
In allowed regions	1.63
Outliers	0
PDB code	3SZ1

R_{sym}, $\Sigma_{hkl;j}$ ($| I_{hkl} - \langle I_{hkl} \rangle |$)/$\Sigma_{hkl;j} I_{hkl}$, where $\langle I_{hkl} \rangle$ is the average intensity for a set of j symmetry-related reflections, and I_{hkl} is the value of the intensity for a single reflection within a set of symmetry-related reflections.
R_{factor}, Σ_{hkl} ($|| F_o | - | F_c ||$)/Σ_{hkl} $| F_o |$, where F_o is the observed structure factor amplitude, and F_c is the calculated structure factor amplitude.
R_{free}, Σ_{hkl},T($|| F_o | - | F_c ||$)/Σ_{hkl} $| F_o |$, where a test set, T (5% of data), is omitted from the refinement.

fold with a small four-stranded β-sheet, as described for other PPARγ structures (Nolte et al., 1998; Li et al., 2008).

It is noteworthy that, as opposed to previous studies in which PPAR ligands preferentially bind to the PPARγ A chain (active configuration) (Itoh et al., 2008), luteolin occupied the LBP of PPARγ chain B (inactive conformation) (Fig. 4). We also detected a second ligand, a long-chain fatty acid simultaneously bound in the chain B LBP, consistent with previous demonstrations that PPARγ can accommodate more than one ligand in the LBP (Itoh et al., 2008; Waku et al., 2010). Because fatty acids were not added during crystallization, we assume that this ligand copurified with the recombinant protein from the bacteria.

Gas chromatography-mass spectrometry analysis of the drops containing the crystals revealed myristic (14:0), palmitic (16:0), and stearic acids (18:0) in the samples (not shown). Myristic acid fits well in the electron density found in chain B. In chain A, electron densities of two fatty acids are also observable but are not as well defined as in chain B. As such, it was only possible to model fatty acids up to nine carbons long in chain A (Fig. 5, C and D), despite the results of the gas chromatography-mass spectrometry experiment. The fatty acid located at H3 and H5 makes hydrophobic contacts with Glu295, Ala292, Arg288, Ser289, Cys285, Phe226, Met329, Ile326, and Leu330 (Fig. 5C), whereas the fatty acid located between H3 and β-sheet makes hydrophobic interactions with Gly259, Arg280, Ile281, Arg288, Ser342, and Ile341 (Fig. 5D).

Luteolin Binds PPARγ in a Different Binding Mode from TZDs. Unlike the TZDs, which adopt a U-shape configuration in the LBP and wrap around H3 to directly contact the activation function 2 helix (H12), luteolin occupies the region of PPARγ delimited by the H3 and the β-sheet and makes no contact with H12, which is displaced in the B-chain (Fig. 4). Despite the fact that luteolin binds in a different mode than rosiglitazone, occupying the region between H3 and β-sheets, A and B rings of luteolin clash with rosiglita-

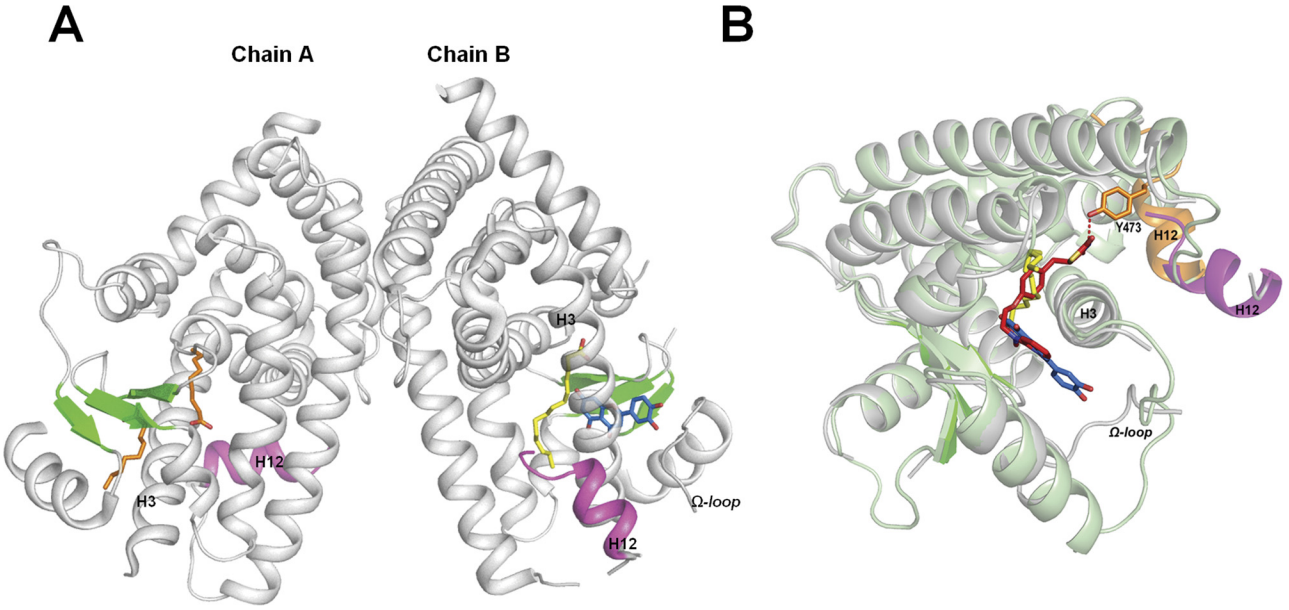

Fig. 4. Structure of PPARγ in complex with luteolin and fatty acids. A, luteolin is blue, myristic acid is yellow, and fatty acids modeled with nine carbons are orange. The Cα atoms of the LBD are magenta (H12), green (β-sheet), and gray (other region). B, superposition of PPARγ in complex with luteolin/myristic acid and PPARγ in complex with rosiglitazone (PDB code 2PRG). 2PRG (pale green) structure presents H12 (orange) in active conformation. Rosiglitazone (red) makes hydrogen bonds with Tyr473 of H12.

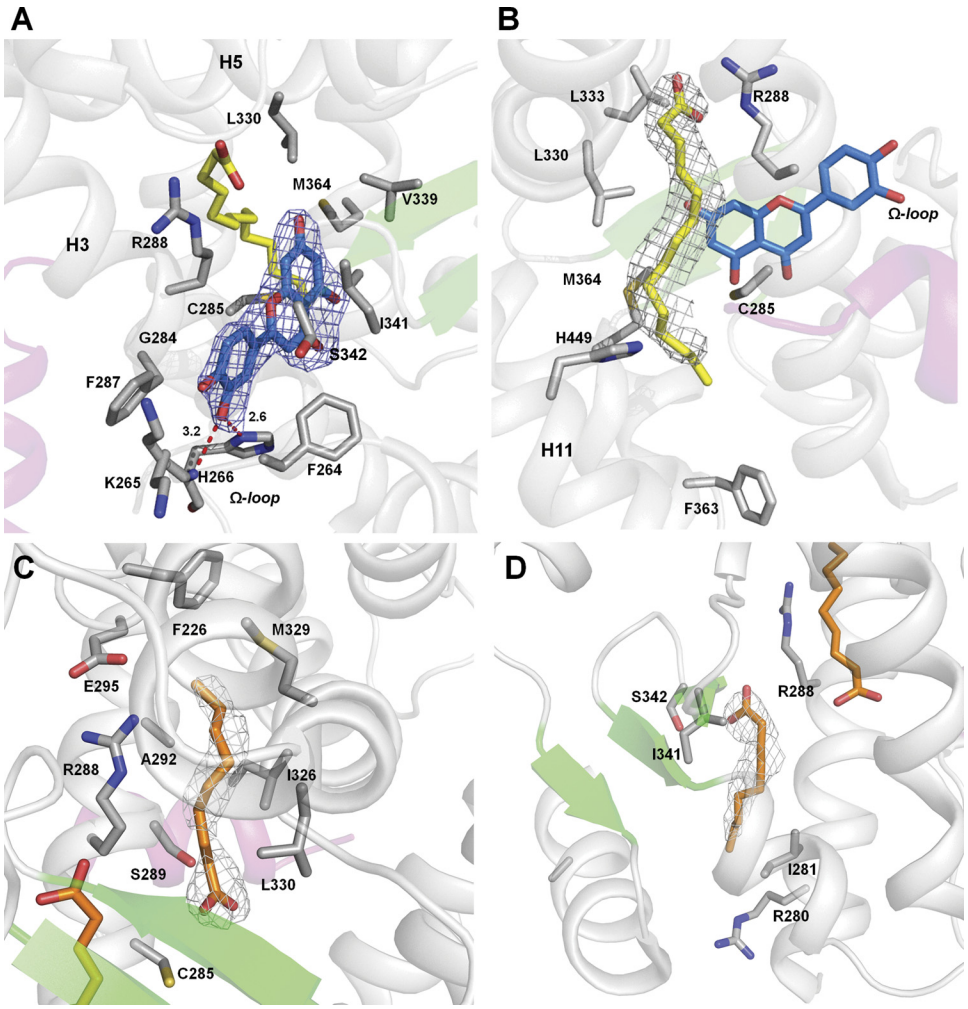

Fig. 5. Ligand-receptor interactions for PPARγ. A σ-weighted $2Fo - F_c$ omit electron-density map is shown contoured at 1.0 σ for the area surrounding ligands. Luteolin (blue) (A), myristic acid (yellow) (B), and fatty acids of chain A (C and D) are shown as sticks. The amino acid residues that interact with the ligands are labeled and show as sticks. H12 is shown in magenta and the β-sheet in green.

zone when our structure was superposed with that in PDB entry 2PRG (Fig. 4B). Luteolin makes two hydrogen bonds with the main chain of the residue Lys265 and the side chain of His266, both located at the Ω-loop that links H2 to H3 and also makes important hydrophobic interactions with Phe264, Gly284, Phe287, Cys285, Arg288, Leu330, Ser342, Ile341, Met364, and Val339 (Fig. 5A). MD simulations starting from this crystallographic structure showed that the binding mode of luteolin is quite stable, and it exhibits only local fluctuations, with root-mean-square deviation of 0.6 ± 0.2 Å. Moreover, the simulations also revealed that an additional hydrogen bond not evident in the structure could be established between luteolin and residue Glu291 (H3), which could help to anchor luteolin to the Ω-loop (Fig. 6). Myristic acid, in turn, occupies the region of the LBD composed of H3, H5, and H7 and makes a salt bridge with Arg288 (H3), with its aliphatic chain surrounded by the residues Ser289, Cys285, Leu330, Leu333, Met364, Phe363, and His449 (Fig. 5B).

MD simulations provide further insights into the binding mode. A water molecule bridges luteolin and the carboxylate of the myristic acid through another hydrogen bond (Fig. 6) and is relatively stable; it is never exchanged with bulk solvent on the time scale of the simulations and seems to be important for anchoring the luteolin in the LBD. It is noteworthy that simultaneous binding of the two ligands seems to be cooperative, because they interact with energy of −11 ± 4 kcal/mol, largely of electrostatic origin. Together, the X-ray structural analysis and the MD simulations suggest that the large binding pocket of the PPARγ LBD makes the simultaneous binding of luteolin and myristic acid possible and that participation of a structural water molecule is involved in the recognition of these ligands.

Rosiglitazone and Luteolin/Myristic Acid Stabilize Different Regions of the LBD. The fact that the luteolin/myristic acid combination binds the LBD in a mode different from that of full agonists raises the possibility that receptor dynamics could be differentially affected by the particular ligand binding mode (Kallenberger et al., 2003; Hamuro et al., 2006). Comparisons of B-factors of our structure, an indication of mobility, and PPARγ with rosiglitazone (PDB code 2PRG) demonstrate that these ligands stabilize different regions. It is noteworthy that luteolin stabilizes Ω-loop, whereas rosiglitazone stabilizes the AF2 helix (Fig. 7A).

We also used MD to compare effects of luteolin/myristic acid and the full agonist rosiglitazone on LBD dynamics. Both simulations used LBD structures in the active configuration. Consistent with the B-factor analysis, the simulations predict that the entire β-sheet region, the Ω-loop and H2′, are preferentially stabilized by luteolin/myristic acid, whereas rosiglitazone preferentially stabilizes H11 and H12 (Fig. 7B). The rosiglitazone-induced stabilization of H12 is explained by a strong H-bond with residue Tyr473 (H12), which is the

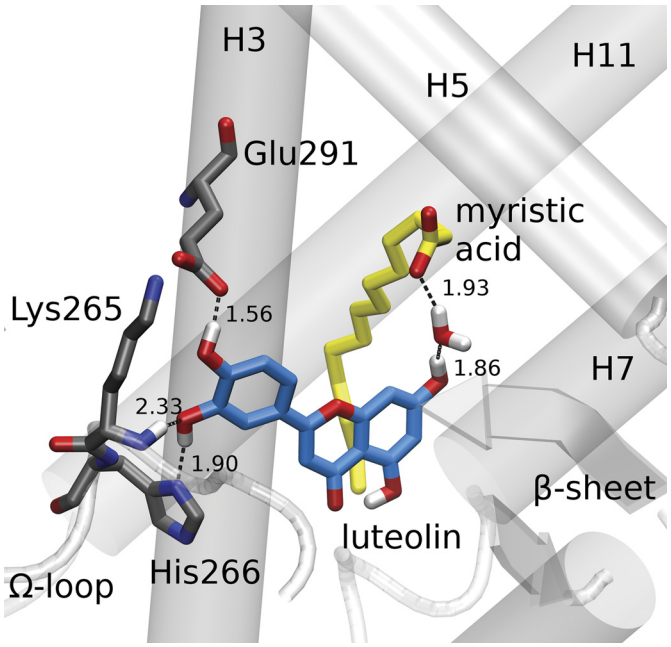

Fig. 6. H-bonds involving luteolin and myristic acid. The two H-bonds between luteolin and the LBD residues Lys265 and His266 seen in the crystallographic structure are very stable according to the simulations. Another hydrogen bond with Glu291, not evident from the X-ray data, is formed during the dynamics, which could help in the stabilization of the luteolin interactions. In addition, a water-mediated hydrogen bond between the luteolin and the myristic acid is shown. This water molecule never exchanges with the bulk solvent and seems to be structurally important for the particular binding mode of luteolin.

structural basis of its agonist behavior (Nolte et al., 1998). In contrast, we found three reasons for the enhanced ligand-induced stabilization of the β-sheet region by luteolin and myristic acid relative to rosiglitazone. First, residue His266 (Ω-loop) is kept rigid as a result of an important H-bond with luteolin and is free to turn to the solvent in the presence of rosiglitazone. In fact, the part of the Ω-loop that is stabilized by luteolin is not seen in chain A of the structure, where luteolin is absent, consistent with a role in stabilization of Ω-loop dynamics. Second, residues Ser342 (β-strand 3) and Lys263 (H2′) are hydrogen-bonded throughout almost the entire simulation when the luteolin is bound to the LBD, which also results in the H2′/Ω-loop stabilization (Figs. 7, C and D). In the presence of rosiglitazone, on the contrary, this configuration is never established. Thus, besides binding to and stabilizing the Ω-loop, luteolin is able to induce the formation of protein-protein interactions in the LBD that contribute to H2′/Ω-loop stabilization. Third, luteolin and myristic coordinate binding of two water molecules that are tightly bound to the backbone of the residues Leu340 and Ser342, both located at the β-sheet (Fig. 7E). So, in addition to the hydrophobic contacts between the aromatic rings of luteolin and the side chains of residues of the β-sheet, water-mediated hydrogen bonds may be important for the stabilization of the β-sheet relative to rosiglitazone complex, in which no immobilized water molecules bind to residues of the β-sheet. Thus, luteolin adopts a different binding mode from TZDs and selectively stabilize different regions of the LBD.

Luteolin Promotes Decrease in Production of IL-8 after Hypertonic Challenge. Because PPARγ overexpression in mice reduced inflammatory and fibrotic responses in corneas subsequent to injury, we used HCECs to assess whether luteolin could suppress injury induced by hypertonic stress, which frequently occurs in dry-eye disease (see *Introduction*), and can trigger increases in IL-8 release by resident cells in the corneal epithelium and the underlying stroma (Luo et al., 2005; Li et al., 2006) and reductions in TEER.

We exposed the HCECs to a hypertonic challenge simulating the dry-eye condition and evaluated the effects of luteolin on hypertonic-induced increases in IL-8 release. Figure 8A shows that hypertonic challenge induced a 3.1-fold increase in IL-8 release over 24 h. This rise was obviated by pre-exposing the cells for 30 min to 5 μM luteolin 24 h and partially reversed by exposing the cells to 1 μM luteolin. It is noteworthy that IL-8 production was increased by the PPARγ antagonist GW9662 under isotonic conditions (Fig. 8B), and preincubation with luteolin reversed this effect. Thus, individual effects of luteolin and GW9662 on IL-8 release are attributable to their respective partial activation and suppression of PPARγ activity.

Finally, we determined whether luteolin modulates the decline in TEER induced by a hypertonic stress. We measured effects on TEER at 375 mOsM because decline of the TEER was not reversible upon restoration of isotonic medium at higher osmolarities (not shown). Figure 9 shows that under the isotonic condition, TEER declined slightly at 5 h, and this effect was reversed completely at 15 h. On the other hand, with the 375 mOsM medium, TEER also fell initially after 5 h without full restoration at 20 h. Pre-exposure to luteolin fully prevented the decline in TEER at 5 h, and the protective effect was also evident at 9 and 20 h.

Discussion

In this work, we investigated the mode of action of luteolin in activating PPARγ by performing functional studies, X-ray crystallography analysis, and molecular dynamics simulations. We found that luteolin exhibits weak partial agonist behavior relative to the full agonist rosiglitazone in cell transactivation assays and that it acts predominantly as an antagonist in gene expression and adipocyte differentiation assays, explaining apparently contradictory results that have suggested that this ligand is an agonist or an antagonist (Mueller et al., 2008; Park et al., 2009; Ding et al., 2010). Our studies also revealed that luteolin exhibits full agonist actions at least one gene in 3T3-L1 cells, *GLUT4*, and acts as a potent anti-inflammatory agent through PPARγ in HCECs. Thus, luteolin also exhibits interesting selective PPARγ modulator actions.

The crystallographic structure is consistent with the idea that luteolin is a weak partial agonist with antagonist actions and also suggests similarities between binding modes of luteolin and other SPPARγMs. Luteolin preferentially binds the nominally inactive B-chain subunit of the PPARγ crystallographic dimer. This is distinct from other PPARγ ligands with full agonist character or partial agonists, which either bind exclusively to the A-chain or occupy both subunits, but are well defined in the A-chain LBP and poorly resolved in the context of the B-chain (Itoh et al., 2008). Second, luteolin is far from H12; this, coupled with B-factor measurements and MD simulations, which indicate that H12 is poorly tethered, suggest that H12 will be highly dynamic and able to adopt active and inactive conformations in the presence of

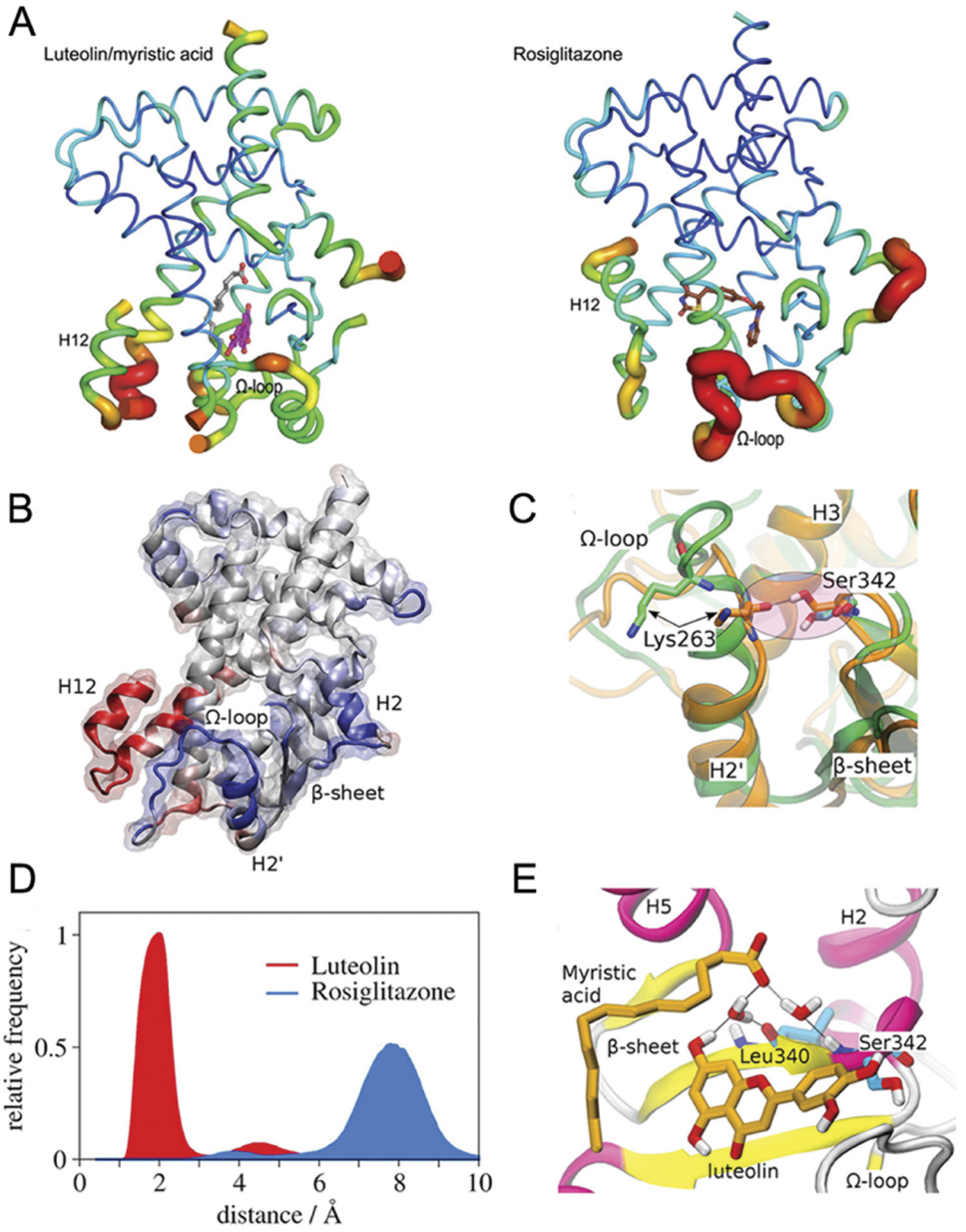

Fig. 7. Ligand-induced stabilization of Ω-loop/β-sheet region. A, B-factors of PPARγ_LBD in complex with rosiglitazone (PDB code 2PRG) and with luteolin/myristic acid. The thickness of the schematic representation is directly proportional to the temperature factors of the region. In the structure with rosiglitazone, the H12 is the active state, and in the structure of luteolin/myristic acid, it is in an inactive state as a result of crystallographic contacts. Luteolin (magenta), myristic acid (gray), and rosiglitazone (brown) are shown as sticks. B, the LBD structure colored according to the mobility as measured by the average root-mean-square deviation of the α carbons. The blue regions are those that are more stabilized by luteolin/myristic acid than by rosiglitazone; the red regions are those stabilized by rosiglitazone relative to luteolin/myristic acid. The β-sheet region is more stabilized by luteolin, whereas rosiglitazone, being a full agonist, preferentially stabilizes H11 and H12. C, a snapshot of the simulations of PPARγ bound to luteolin (orange) and to rosiglitazone (green) showing the spatial configurations of the residues Lys263 and Ser342, which are kept in contact in the presence of luteolin, contributing to the stabilization of the H2′ and Ω-loop region. D, the distributions of the distance between the residues Lys263 and Ser342 in the presence of luteolin and rosiglitazone, showing the differences between the ligand-induced effects on this region. E, the H-bond network involving luteolin, myristic acid, Leu340, Ser342, and two water molecules. These water molecules bind the two ligands to the β-sheet and are never seen exchanging with the bulk solvent during the course of the simulations.

luteolin. Luteolin also binds close to, and strongly stabilizes, the H3/β-sheet region of the LBD (Fig. 4), similar to PPARγ partial agonists, which act as preferential insulin sensitizers (Bruning et al., 2007), inhibit cyclin-dependent kinase 5-dependent phosphorylation, and exhibit insulin-sensitizing effects without harmful side effects in animal models (Choi et al., 2010; Choi et al., 2011). Luteolin has documented beneficial effects on blood glucose and insulin sensitivity, similar to SPPARγMs (Berger et al., 2003; Acton et al., 2005; Liu et al., 2005) and inhibits PPARγ adipogenic activity (Park et al., 2009) while potentiating insulin action in adipocytes (Ding et al., 2010) and endothelium (Deqiu et al., 2011). It is therefore interesting to suggest that desirable properties may relate to the binding position of luteolin in the LBP.

Our structure reveals myristic acid, probably bacterial in origin, in the LBP along with luteolin. Previous studies have shown that the PPARγ LBP can accommodate more than one ligand (Waku et al., 2010). Although this raises the possibility that PPARγ may sense a phytochemical and a fatty acid (or, perhaps, other combinations of signaling molecules), we have not been able to obtain any evidence that myristic acid alters luteolin activities through PPARγ in transfections (not shown). However, our MD simulations do suggest that luteolin and myristic acid cooperate to stabilize the Ω-loop, which links H2′ to H3, explaining why it is visible in our structure even though it is often impossible to resolve, irrespective of ligand type. Furthermore, comparison of B-factors in the presence of luteolin/myristic acid and rosiglitazone (PDB code 2PRG) indicates that luteolin preferentially stabilizes Ω-loop and β-sheet (Fig. 7A), whereas rosiglitazone preferentially stabilizes H12 (Fig. 7B) because of a strong H-bond with the residue Tyr473 (H12) (Fig. 4B) (Nolte et al., 1998). MD simulations indicate that luteolin and myristic acid are both involved in the preferential stabilization of the entire β-sheet region of the LBD, including Ω-loop and H2′. This is related to a strong H-bond with His266 (Ω-loop), which is free to turn to solvent in the presence of rosiglitazone; residues Ser342 (β-strand 3) and Lys263 (H2′) remain hydrogen-

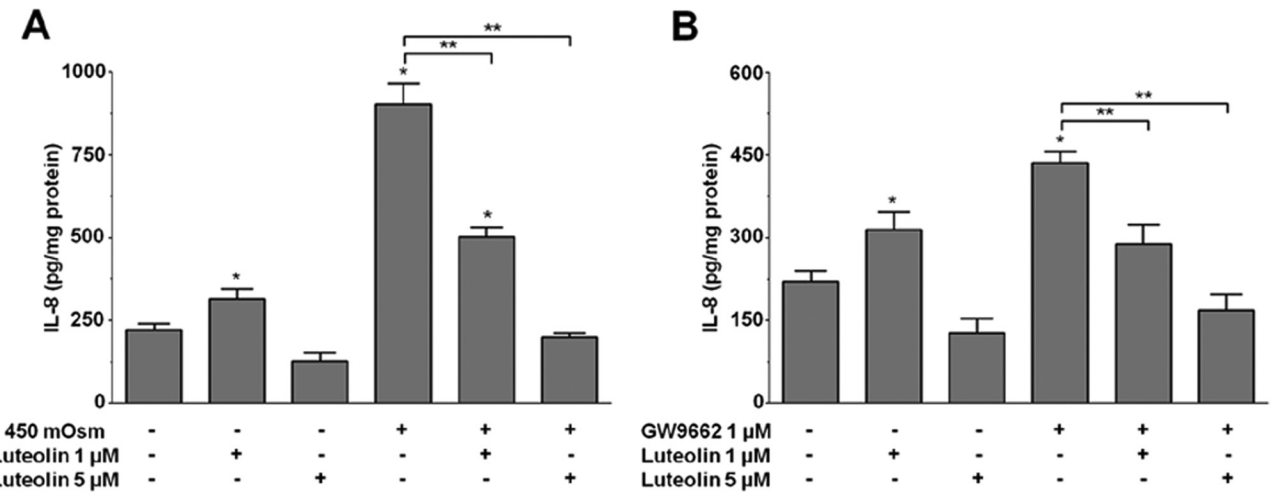

Fig. 8. A, luteolin reverses hypertonic-induced increases in IL-8 release: HCECs were cultured in multiwell plates for 24 h in the presence and absence of 5 μM luteolin. When luteolin was used, the cells were pre-exposed to this PPARγ agonist luteolin for 30 min before substituting the isotonic (i.e., 300 mOsM) medium with a 450 mOsM hypertonic counterpart. ELISA was used to measure IL-8 release into the medium. Each experiment was performed three times in triplicate (*, significant under isotonic conditions between values in the presence and absence of luteolin; **, significant under hypertonic conditions between values in the presence and absence of luteolin. *, **, $P < 0.05$, values are expressed as mean ± S.E.M.). B, luteolin reverses GW9662-induced increases in IL-8 release: HCECs were cultured in multiwell plates and pre-exposed to 1 μM GW9662 for 30 min before adding 1 or 5 μM luteolin in isotonic medium. ELISA measured IL-8 release into the medium. Each experiment was performed three times in triplicate (*, in isotonic medium, significant between values in the presence and absence of luteolin; **, significant between values obtained with GW9662 alone relative to those obtained after exposure to both luteolin and GW9662. ($P < 0.05$, values are expressed as mean± S.E.M.).

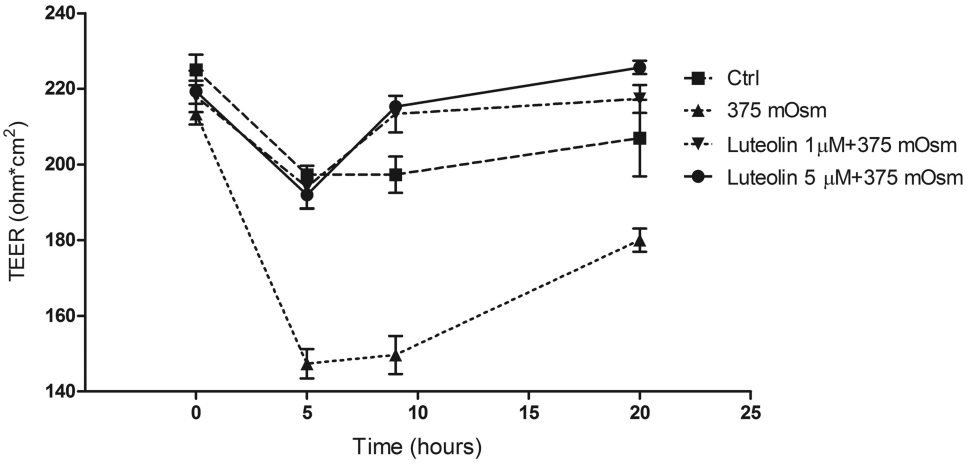

Fig. 9. Luteolin reduces hypertonic-induced TEER declines. HCECs were cultured in transwell plates and incubated in 1 or 5 μM luteolin for 30 min, and then were exposed to either 375 mOsM medium or isotonic medium for 20 h. TEER was measured at the indicated times. Data are shown as means ± S.E.M. of triplicate measurements from three different experiments for each condition. Either 1 or 5 μM luteolin fully protected HCECs from declines in TEER induced by exposure to 375 mOsM medium. *, $P < 0.05$, versus the corresponding value for cells incubated with isotonic medium.

bonded throughout almost the whole simulation time; and luteolin and myristic acid have the ability to coordinate two molecules of water tightly bound to the backbone of residues Leu340 and Ser342, both located at the β-sheet (Fig. 7E). The aromatic rings of luteolin also make hydrophobic interactions on the β-sheet, at residues such as Val339, Ile341, and Ser342, and MD simulations also reveal a water-mediated hydrogen bond with Ser342.

The significance of Ω-loop stabilization is not clear. There are precedents for ligand interaction with the Ω-loop; ajulemic acid, a synthetic cannabinoid that lacks hallucinogenic activities and is a partial PPARγ agonist also makes polar contacts with the main chain of Lys265 and His266 and extensive hydrophobic contacts with the side chain of Phe264 (Ambrosio et al., 2007). Previous studies suggested that fatty acid metabolites activate PPARγ through structural rearrangements of the Ω-loop and that distinct degrees of the receptor activities in cells are derived from structural differences in this region (Waku et al., 2009). Because luteolin also seems particularly ineffective at stabilizing H12, it is interesting to suggest that its weak partial agonist and gene-specific agonist actions may derive from a mechanism distinct from full agonists and that the β-sheets and Ω-loop participate in these effects (Bruning et al., 2007).

Finally, even though luteolin is a weak partial agonist, it exhibits strong anti-inflammatory potential in the corneal epithelial and endothelial layers, and this suggests that it may have therapeutic value in ocular diseases (Sarayba et al., 2005). Flavonoids are known to exhibit anti-inflammatory activities (Havsteen, 2002), and we have shown here that luteolin reverts the hypertonic-induced increase in IL-8 in HCECs through PPARγ, as indicated by the ability of luteolin to reverse decreased IL-8 production induced by PPARγ antagonist GW9662. Luteolin can also provide a protective effect against declines in TEER induced by exposure to 375 mOsM medium. We cannot yet explain anti-inflammatory actions in terms of effects on PPARγ structure and dynamics, but our structure does suggest that anti-inflammatory actions must be independent of full H12 stabilization. Thus, protective effects rendered against hypertonic induced

increases in IL-8 release by HCECs and accompanying declines in epithelial barrier function by luteolin suggest that a weak partial PPARγ agonist, with possibly a safer profile than full PPARγ agonists, will exhibit useful effects in eye disease and injury-induced inflammation. In summary, PPARγ may be a novel therapeutic target for treating dry-eye patients, and the fact that luteolin, with a unique binding mode and activity profile relative to TZDs, exhibits efficacy in this system suggests that it should be possible to elicit such actions with safe partial agonists or SPPARMγ ligands that lack full agonist activity.

Acknowledgments

We thank Dr. João Renato Carvalho Muniz and José Fernando Ruggiero Bachega for scientific discussions. We are also grateful to the Brazilian National Synchrotron Light Laboratory (LNLS, Campinas, Brazil) for the use of the MX-2 beamline.

Authorship Contributions

Participated in research design: Puhl, Bernardes, Silveira, Yuan, Reinach, Skaf, and Polikarpov.

Conducted experiments: Puhl, Bernardes, Silveira, Yuan, Campos, Saidemberg, and Ayers.

Contributed new reagents or analytical tools: Palma and Polikarpov.

Performed data analysis: Puhl, Bernardes, Silveira, Yuan, Campos, Saidemberg, Cvoro, and Reinach.

Wrote or contributed to the writing of the manuscript: Puhl, Bernardes, Silveira, Yuan, Webb, Reinach, Skaf, and Polikarpov.

References

Acton JJ 3rd, Black RM, Jones AB, Moller DE, Colwell L, Doebber TW, Macnaul KL, Berger J, and Wood HB (2005) Benzoyl 2-methyl indoles as selective PPARgamma modulators. *Bioorg Med Chem Lett* **15:**357–362.

Adams PD, Afonine PV, Bunkóczi G, Chen VB, Davis IW, Echols N, Headd JJ, Hung LW, Kapral GJ, Grosse-Kunstleve RW, et al. (2010) PHENIX: a comprehensive Python-based system for macromolecular structure solution. *Acta Crystallogr D Biol Crystallogr* **66:**213–221.

Ambrosio AL, Dias SM, Polikarpov I, Zurier RB, Burstein SH, and Garratt RC (2007) Ajulemic acid, a synthetic nonpsychoactive cannabinoid acid, bound to the ligand binding domain of the human peroxisome proliferator-activated receptor gamma. *J Biol Chem* **282:**18625–18633.

Armoni M, Harel C, and Karnieli E (2007) Transcriptional regulation of the GLUT4 gene: from PPAR-gamma and FOXO1 to FFA and inflammation. *Trends Endocrinol Metab* **18:**100–107.

Auwerx J (1999) PPARgamma, the ultimate thrifty gene. *Diabetologia* **42:**1033–1049.

Berger J and Moller DE (2002) The mechanisms of action of PPARs. *Annu Rev Med* **53:**409–435.

Berger JP, Petro AE, Macnaul KL, Kelly LJ, Zhang BB, Richards K, Elbrecht A, Johnson BA, Zhou G, Doebber TW, et al. (2003) Distinct properties and advantages of a novel peroxisome proliferator-activated protein [gamma] selective modulator. *Mol Endocrinol* **17:**662–676.

Borniquel S, Jansson EA, Cole MP, Freeman BA, and Lundberg JO (2010) Nitrated oleic acid up-regulates PPARgamma and attenuates experimental inflammatory bowel disease. *Free Radic Biol Med* **48:**499–505.

Bruning JB, Chalmers MJ, Prasad S, Busby SA, Kamenecka TM, He Y, Nettles KW, and Griffin PR (2007) Partial agonists activate PPARgamma using a helix 12 independent mechanism. *Structure* **15:**1258–1271.

Choi JH, Banks AS, Estall JL, Kajimura S, Boström P, Laznik D, Ruas JL, Chalmers MJ, Kamenecka TM, Blüher M, et al. (2010) Anti-diabetic drugs inhibit obesity-linked phosphorylation of PPARgamma by Cdk5. *Nature* **466:**451–456.

Choi JH, Banks AS, Kamenecka TM, Busby SA, Chalmers MJ, Kumar N, Kuruvilla DS, Shin Y, He Y, Bruning JB, et al. (2011) Antidiabetic actions of a non-agonist PPARγ ligand blocking Cdk5-mediated phosphorylation. *Nature* **477:**477–481.

Chui PC, Guan HP, Lehrke M, and Lazar MA (2005) PPARgamma regulates adipocyte cholesterol metabolism via oxidized LDL receptor 1. *J Clin Invest* **115:**2244–2256.

Collaborative Computational Project Number 4 (1994) The CCP4 suite: programs for protein crystallography. *Acta Crystallogr D Biol Crystallogr* **50:**760–763.

Deqiu Z, Kang L, Jiali Y, Baolin L, and Gaolin L (2011) Luteolin inhibits inflammatory response and improves insulin sensitivity in the endothelium. *Biochimie* **93:**506–512.

Ding L, Jin D, and Chen X (2010) Luteolin enhances insulin sensitivity via activation of PPARγ transcriptional activity in adipocytes. *J Nutr Biochem* **21:**941–947.

Emsley P and Cowtan K (2004) Coot: model-building tools for molecular graphics. *Acta Crystallogr D Biol Crystallogr* **60:**2126–2132.

Frisch MJ, Trucks GW, Schlegel HB, Scuseria GE, Robb MA, Cheeseman JR, Montgomery JA Jr, Vreven T, Kudin KN, Burant JC, et al. (2004) *Gaussian 03 Revision E01*, Gaussian, Wallingford CT.

Gampe RT Jr, Montana VG, Lambert MH, Miller AB, Bledsoe RK, Milburn MV, Kliewer SA, Willson TM, and Xu HE (2000) Asymmetry in the PPARgamma/RXRalpha crystal structure reveals the molecular basis of heterodimerization among nuclear receptors. *Mol Cell* **5:**545–555.

Giaginis C, Giagini A, and Theocharis S (2009) Peroxisome proliferator-activated receptor-gamma (PPAR-gamma) ligands as potential therapeutic agents to treat arthritis. *Pharmacol Res* **60:**160–169.

Guimarães BG, Sanfelici L, Neuenschwander RT, Rodrigues F, Grizolli WC, Raulik MA, Piton JR, Meyer BC, Nascimento AS, and Polikarpov I (2009) The MX2 macromolecular crystallography beamline: a wiggler X-ray source at the LNLS. *J Synchrotron Radiat* **16:**69–75.

Hamuro Y, Coales SJ, Morrow JA, Molnar KS, Tuske SJ, Southern MR, and Griffin PR (2006) Hydrogen/deuterium-exchange (H/D-Ex) of PPARgamma LBD in the presence of various modulators. *Protein Sci* **15:**1883–1892.

Hansson A, Souza PC, Silveira RL, Martínez L, and Skaf MS (2011) CHARMM force field parametrization of rosiglitazone. *Int J Quantum Chem* **111:**1346–1354.

Havsteen BH (2002) The biochemistry and medical significance of the flavonoids. *Pharmacol Ther* **96:**67–202.

Higgins LS and Depaoli AM (2010) Selective peroxisome proliferator-activated receptor gamma (PPARgamma) modulation as a strategy for safer therapeutic PPARgamma activation. *Am J Clin Nutr* **91:**267S–272S.

Itoh T, Fairall L, Amin K, Inaba Y, Szanto A, Balint BL, Nagy L, Yamamoto K, and Schwabe JW (2008) Structural basis for the activation of PPARgamma by oxidized fatty acids. *Nat Struct Mol Biol* **15:**924–931.

Jorgensen WL, Chandrasekhar J, Madura JD, Impey RW, and Klein ML (1983) Comparison of simple potential functions for simulating liquid water. *J Chem Physics* **79:**926–935.

Kallenberger BC, Love JD, Chatterjee VK, and Schwabe JW (2003) A dynamic mechanism of nuclear receptor activation and its perturbation in a human disease. *Nat Struct Biol* **10:**136–140.

Klemm DJ, Leitner JW, Watson P, Nesterova A, Reusch JE, Goalstone ML, and Draznin B (2001) Insulin-induced adipocyte differentiation. Activation of CREB rescues adipogenesis from the arrest caused by inhibition of prenylation. *J Biol Chem* **276:**28430–28435.

Kliewer SA, Lenhard JM, Willson TM, Patel I, Morris DC, and Lehmann JM (1995) A prostaglandin J2 metabolite binds peroxisome proliferator-activated receptor gamma and promotes adipocyte differentiation. *Cell* **83:**813–819.

Koshiyama H, Shimono D, Kuwamura N, Minamikawa J, and Nakamura Y (2001) Rapid communication: inhibitory effect of pioglitazone on carotid arterial wall thickness in type 2 diabetes. *J Clin Endocrinol Metab* **86:**3452–3456.

Laplante M, Sell H, MacNaul KL, Richard D, Berger JP, and Deshaies Y (2003) PPAR-gamma activation mediates adipose depot-specific effects on gene expression and lipoprotein lipase activity: mechanisms for modulation of postprandial lipemia and differential adipose accretion. *Diabetes* **52:**291–299.

Larsen TM, Toubro S, and Astrup A (2003) PPARgamma agonists in the treatment of type II diabetes: is increased fatness commensurate with long-term efficacy? *Int J Obes Relat Metab Disord* **27:**147–161.

Lehmann JM, Lenhard JM, Oliver BB, Ringold GM, and Kliewer SA (1997) Peroxisome proliferator-activated receptors alpha and gamma are activated by indomethacin and other non-steroidal anti-inflammatory drugs. *J Biol Chem* **272:**3406–3410.

Lehmann JM, Moore LB, Smith-Oliver TA, Wilkison WO, Willson TM, and Kliewer SA (1995) An antidiabetic thiazolidinedione is a high affinity ligand for peroxisome proliferator-activated receptor gamma (PPAR gamma). *J Biol Chem* **270:**12953–12956.

Lehrke M and Lazar MA (2005) The many faces of PPARgamma. *Cell* **123:**993–999.

Leslie AG (1999) Integration of macromolecular diffraction data. *Acta Crystallogr D Biol Crystallogr* **55:**1696–1702.

Lewis JD, Lichtenstein GR, Stein RB, Deren JJ, Judge TA, Fogt F, Furth EE, Demissie EJ, Hurd LB, Su CG, et al. (2001) An open-label trial of the PPARgamma ligand rosiglitazone for active ulcerative colitis. *Am J Gastroenterol* **96:**3323–3328.

Li DQ, Luo L, Chen Z, Kim HS, Song XJ, and Pflugfelder SC (2006) JNK and ERK MAP kinases mediate induction of IL-1beta, TNF-alpha and IL-8 following hyperosmolar stress in human limbal epithelial cells. *Exp Eye Res* **82:**588–596.

Li Y, Zhang J, Schopfer FJ, Martynowski D, Garcia-Barrio MT, Kovach A, Suino-Powell K, Baker PR, Freeman BA, Chen YE, et al. (2008) Molecular recognition of nitrated fatty acids by PPAR gamma. *Nat Struct Mol Biol* **15:**865–867.

Liu K, Black RM, Acton JJ 3rd, Mosley R, Debenham S, Abola R, Yang M, Tschirret-Guth R, Colwell L, Liu C, et al. (2005) Selective PPARgamma modulators with improved pharmacological profiles. *Bioorg Med Chem Lett* **15:**2437–2440.

Luo L, Li DQ, Corrales RM, and Pflugfelder SC (2005) Hyperosmolar saline is a proinflammatory stress on the mouse ocular surface. *Eye Contact Lens* **31:**186–193.

MacKerell AD, Bashford D, Bellott M, Dunbrack RL, Evanseck JD, Field MJ, Fischer S, Gao J, Guo H, Ha S, et al. (1998) All-atom empirical potential for molecular modeling and dynamics studies of proteins. *J Phys Chem B* **102:**3586–3616.

Martínez L, Andreani R, and Martínez JM (2007) Convergent algorithms for protein structural alignment. *BMC Bioinformatics* **8:**306.

Morrison RF and Farmer SR (1999) Insights into the transcriptional control of adipocyte differentiation. *J Cell Biochem* **Suppl 32–33:**59–67.

Mudaliar S, Chang AR, and Henry RR (2003) Thiazolidinediones, peripheral edema, and type 2 diabetes: incidence, pathophysiology, and clinical implications. *Endocr Pract* **9:**406–416.

Mueller M, Lukas B, Novak J, Simoncini T, Genazzani AR, and Jungbauer A (2008) Oregano: a source for peroxisome proliferator-activated receptor gamma antagonists. *J Agric Food Chem* **56:**11621–11630.

Nissen SE and Wolski K (2007) Effect of rosiglitazone on the risk of myocardial infarction and death from cardiovascular causes. *N Engl J Med* **356:**2457–2471.
Nolte RT, Wisely GB, Westin S, Cobb JE, Lambert MH, Kurokawa R, Rosenfeld MG, Willson TM, Glass CK, and Milburn MV (1998) Ligand binding and co-activator assembly of the peroxisome proliferator-activated receptor-gamma. *Nature* **395:** 137–143.
Park HS, Kim SH, Kim YS, Ryu SY, Hwang JT, Yang HJ, Kim GH, Kwon DY, and Kim MS (2009) Luteolin inhibits adipogenic differentiation by regulating PPARgamma activation. *Biofactors* **35:**373–379.
Phillips JC, Braun R, Wang W, Gumbart J, Tajkhorshid E, Villa E, Chipot C, Skeel RD, Kalé L, and Schulten K (2005) Scalable molecular dynamics with NAMD. *J Comput Chem* **26:**1781–1802.
Ricote M and Glass CK (2007) PPARs and molecular mechanisms of transrepression. *Biochim Biophys Acta* **1771:**926–935.
Ricote M, Huang J, Fajas L, Li A, Welch J, Najib J, Witztum JL, Auwerx J, Palinski W, and Glass CK (1998) Expression of the peroxisome proliferator-activated receptor gamma (PPARgamma) in human atherosclerosis and regulation in macrophages by colony stimulating factors and oxidized low density lipoprotein. *Proc Natl Acad Sci USA* **95:**7614–7619.
Saika S, Yamanaka O, Okada Y, Miyamoto T, Kitano A, Flanders KC, Ohnishi Y, Nakajima Y, Kao WW, and Ikeda K (2007) Effect of overexpression of PPARgamma on the healing process of corneal alkali burn in mice. *Am J Physiol Cell Physiol* **293:**C75–C86.
Sarayba MA, Li L, Tungsiripat T, Liu NH, Sweet PM, Patel AJ, Osann KE, Chittiboyina A, Benson SC, Pershadsingh HA, et al. (2005) Inhibition of corneal neovascularization by a peroxisome proliferator-activated receptor-gamma ligand. *Exp Eye Res* **80:**435–442.
Singh UC and Kollman PA (1984) An approach to computing eletrostatic charges for molecules. *J Comput Chem* **5:**129–145.
Tontonoz P, Hu E, Graves RA, Budavari AI, and Spiegelman BM(1994) mPPAR gamma 2: tissue-specific regulator of an adipocyte enhancer. *Genes Dev* **8:**1224–1234.
Waku T, Shiraki T, Oyama T, Fujimoto Y, Maebara K, Kamiya N, Jingami H, and Morikawa K (2009) Structural insight into PPARgamma activation through covalent modification with endogenous fatty acids. *J Mol Biol* **385:**188–199.
Waku T, Shiraki T, Oyama T, Maebara K, Nakamori R, and Morikawa K (2010) The nuclear receptor PPARγ individually responds to serotonin- and fatty acid-metabolites. *EMBO J* **29:**3395–3407.
Xagorari A, Papapetropoulos A, Mauromatis A, Economou M, Fotsis T, and Roussos C (2001) Luteolin inhibits an endotoxin-stimulated phosphorylation cascade and proinflammatory cytokine production in macrophages. *J Pharmacol Exp Ther* **296:**181–187.
Yang H, Reinach PS, Koniarek JP, Wang Z, Iserovich P, and Fischbarg J (2000) Fluid transport by cultured corneal epithelial cell layers. *Br J Ophthalmol* **84:**199–204.
Zoete V, Grosdidier A, and Michielin O (2007) Peroxisome proliferator-activated receptor structures: ligand specificity, molecular switch and interactions with regulators. *Biochim Biophys Acta* **1771:**915–925.

Address correspondence to: Igor Polikarpov, Departamento de Física e Informática, Instituto de Física de São Carlos, Universidade de São Paulo. Av. Trabalhador Sãocarlense, no. 400, São Carlos-SP, Zip Code 13.566-590, Brazil. E-mail: ipolikarpov@ifsc.usp.br